EURASIAN PHYSICAL TECHNICAL JOURNAL

2024, Volume 21, No. 3 (49)

https://doi.org/10.31489/2024No3/99-107

Received: 29/06/2024 Revised: 11/09/2024 Accepted: 19/09/2024 Published online: 30/09/2024

Research Article

UDC 549.641.1, 620.3

EFFECT OF ANNEALING DURATION ON PHOTOCATALYTIC PROPERTIES OF $LaFeO_3$ PEROVSKITE

Zhanbirbayeva P.A., Baltabekov A.S., Kayumova A.S., Kuanyshbekova A.B., Adambay T.N., Serikov T.M. *

E.A. Buketov, Karaganda University, Karaganda, Kazakhstan
*Corresponding authors: serikov-timur@mail.ru

Abstract. *In this paper, the effect of the annealing duration on the photocatalytic properties of lanthanum ferrite perovskite synthesized by the hydrothermal method is investigated. Lanthanum ferrite was chosen as the object of study due to its high activity under the influence of visible light. During the experiments, the structural changes occurring in the material during annealing during 2, 4 and 6 hours were studied. The main attention was paid to the analysis of the morphology of nanoparticles, phase composition, crystallinity, absorption spectra and photocatalytic activity. The results show that an increase in the annealing time leads to an improvement in the crystal structure, an increase in the size of crystallites and a higher level of oxygenation. The optimal annealing time to achieve maximum photocatalytic activity was determined to be 6 hours. The work confirms the prospects of using long-term annealing to improve the photocatalytic properties of perovskite-based materials.*

Keywords: Lanthanum ferrite, annealing duration, photocatalytic activity.

1. Introduction

Currently, solar energy, as a bright and renewable source, is used as an alternative to fossil fuels [1]. Photocatalysis is a promising environmentally friendly method based on the use of semiconductor photocatalysts with high chemical and thermal stability. These processes are usually carried out with the participation of photoinduced charge carriers under mild operating conditions without the addition of chemicals. This gives photocatalysis an advantage over traditional methods such as biological and electrocatalytic treatment, which are often accompanied by instability, low mechanical strength, poisoning of catalysts and corrosion of electrodes [2,3]. The use of solar energy by semiconductor photocatalysts makes it possible to obtain hydrogen by reducing water, convert CO_2 into useful chemicals and oxidize various pollutants [4]. Thus, semiconductor-based photocatalysis is considered as a clean, cost-effective, renewable and safe technology [5]. Since the first report on photocatalysis using TiO_2 [6], this area has attracted considerable attention from scientists around the world. To date, there are many semiconductor photocatalysts, such as ZnO [7], SnO_2 [8], $BiVO_4$ [9], BiOCl [10], $SrTiO_3$ [11], WO_3 [12], Fe_2O_3 [13], Ta_2O_5 [14], $BiFeO_3$ [15], Bi_2WO_6 [16], Cu_2O [17], g-C_3N_4 [18], graphene [19] and carbon nanotubes [20] are actively used in the photocatalytic production of solar fuels and environmental purification.

Many promising environmentally friendly methods have been developed for photocatalytic disinfection of water and reduction of CO_2 emissions aimed at use in green and renewable energy [21]. During the process of semiconductor photocatalysis, highly reactive and transient particles are generated on the surface of a semiconductor material when it is exposed to light with a wavelength corresponding to or exceeding the band gap of the substance [22]. These particles exhibit a remarkable capacity for oxidation and reduction, enabling

them to break down pollutants, mitigate CO_2 emissions, and facilitate the splitting of water [23]. Recently, materials such as perovskites have garnered significant attention within the realm of photocatalytic research. Perovskites are crystalline materials with a stable structure of the ABO_3 type, which exhibits remarkable flexibility in its composition. This flexibility arises from the capacity to replace ions of rare-earth or alkaline-earth metals in position A, as well as transition metals in position B. The exceptional properties of perovskites as photocatalysts stem from their ability to manipulate valence and vacancy states, significantly enhancing their catalytic capabilities. Moreover, perovskite-based photocatalytic materials boast a narrow bandgap, enabling more efficient utilization of solar energy compared to other semiconductor-based counterparts [24].

Of particular relevance in this context is the lanthanum ferrite compound, $LaFeO_3$, which exhibits remarkable photocatalytic properties when exposed to visible light with an energy gap of 2.0 eV [25]. Within the perovskite structure of $LaFeO_3$, the rare-earth metal ion assumes position A, while the transition metal cation takes up position B [26].

There are various methods for the synthesis of $LaFeO_3$ nanostructures, which are used in the fields of energy and ecology. These include hydrothermal, solvothermal, sol-gel, microwave, and sonochemical methods. In this study, the hydrothermal method was employed for the synthesis of $LaFeO_3$, as it has several advantages. The hydrothermal method enables the material to be produced at relatively low temperatures, contributing to the formation of high-quality crystalline structures with controlled morphology and a narrow range of particle sizes. This approach also ensures a high degree of uniformity and purity in the sample, which is crucial for subsequent investigations of photocatalytic properties.

This work is aimed at studying the effect of annealing duration on the structural and photocatalytic properties of $LaFeO_3$ synthesized by the hydrothermal method.

2. Experimental part

Synthesis of $LaFeO_3$

During hydrothermal synthesis of $LaFeO_3$: 5 mmol $La(NO_3)_3$ $6H_2O$ and 5 mmol $Fe(NO_3)_3$ $9H_2O$ is dissolved in 10 ml of deionized water. Then 10 mmol of citric acid was added to the mixture and continuously stirred for 2 hours at room temperature. The pH value was adjusted to 9 using ammonium hydroxide, after which the mixture was stirred for another 1 hour. The resulting solution was transferred to a 50 ml Teflon autoclave and heated at 180 ° C for 12 hours. The solids were separated by centrifugation, washed with deionized water and ethanol, dried at 80 °C for 5 hours, and then calcined in air at 800 °C for 2, 4 and 6 hours.

The morphology of nanocomposite materials was studied using the Mira scanning electron microscope in 3 LMU (Tuscan), which is based on the energy dispersion analysis (EDA) function. The images of Pam, Pam paintings and Said were obtained using a transmission electron microscope DSR-1400 plus (JEOL) with an accelerating voltage of 120 kV. The phase composition of the samples was studied using X-ray diffraction on an XRD analysis diffractometer (Rigaku Ultima IV). X-ray diffraction analysis was measured using a Confotec MR520 scanning Raman microscope (SOL Instruments, Belarus). The absorption spectra of the studied samples were measured on the CM 2203 device (Solar, Belarus). The specific surface area and pore size of the samples were studied using the ASAP 2460 analyzer. To study the photocatalytic properties, a single-channel potentiostat, the Corrtest CS 350 galvanostat with an integrated FRA module, was used. The photocatalytic activity of the samples was assessed by the response of the photocurrent under artificial sunlight with a 10-second intermittent on/off switch.

3. Results and Discussion

Figure 1 shows images of $LaFeO_3$ nanoparticles obtained using a scanning electron microscope (SEM) synthesized by the hydrothermal method with different annealing durations (2 hours, 4 hours and 6 hours). The formation of microspheres was observed after 2 hours (Fig. 1 a, b), however, few aggregated nanoparticles were observed, which proves that the formation of $LaFeO_3$ microspheres occurs due to the process of self-assembly of nanoparticles [27]. After annealing for 4 hours of $LaFeO_3$ (see Figure 1 d, e), a more uniform particle size distribution is observed, they have a rounded shape and the average size was ~104 nm. The SEM image for the extended reaction time of $LaFeO_3$_6h in Fig. 1g, h shows microspheres with a smooth surface and with an average size of ~110 nm. No cavities or defects were found in the microspheres. The particles have acquired a smoother and more spherical shape, which indicates a further improvement in the crystal structure.

Also depicted in Figure 1 are energy dispersion analysis spectra showing the constituent elements La, Fe and O for each sample. The EDA spectrum of $LaFeO_3$_2h (Figure 1c) shows the percentage of elements: La

— 57%, O — 21.5%, Fe — 21.5%. These data confirm the presence of all the necessary elements in the composition of $LaFeO_3$. And for the $LaFeO_3$_4h sample, the EDA (Figure 1f) spectrum shows a decrease in the La content to 54.5%, an increase in the oxygen content to 25.5% and a decrease in the Fe fraction to 19.9%. This may indicate an improvement in the oxygenation of the structure. As a result of annealing, oxygen atoms can better integrate into the crystal lattice of $LaFeO_3$, which leads to an increase in the oxygen content relative to other elements (lanthanum and iron). In the EDA spectra, we see an increase in the percentage of oxygen as the annealing time increases, which indicates a more complete incorporation of oxygen into the structure of the material. The EDA spectrum of $LaFeO_3$_6h (Figure 1i) shows a further decrease in the La content to 53.2%, an increase in the O content to 26%, and the Fe content is 20.8%. These changes show that long waiting contributed to even more complete oxygenation and crystallization of the material. Oxygenation contributes to the formation and stabilization of the correct crystal structure of perovskite, in which each atom takes its place in the lattice. This is important to ensure uniform charge distribution and improve the photocatalytic properties of the material.

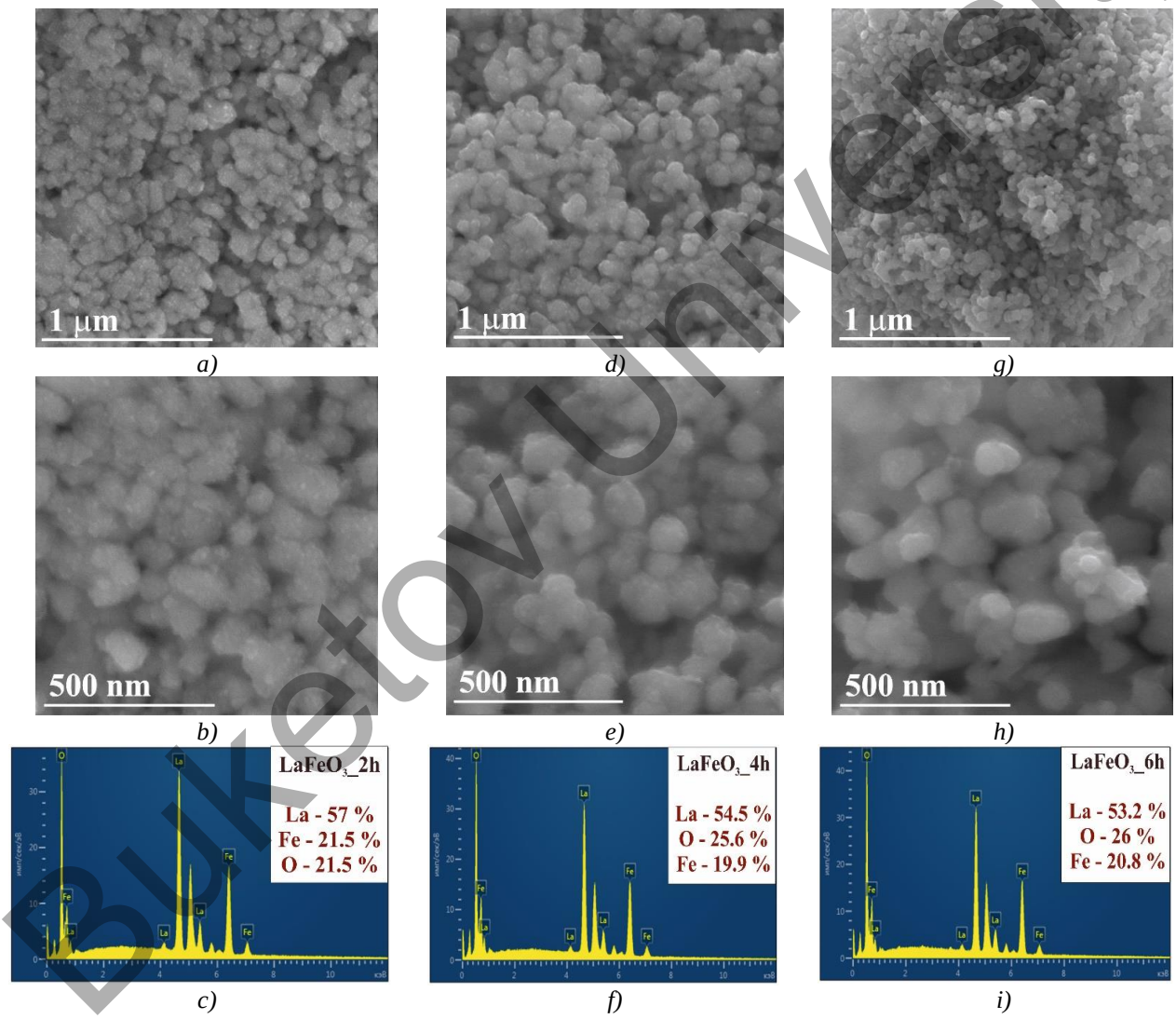

Fig.1. SEM of $LaFeO_3$ perovskite nanoparticles (a,b) $LaFeO_3$_2h, (d,e) $LaFeO_3$_4h, (g,h) $LaFeO_3$_6h and EDA (c) $LaFeO_3$_2h, (f) $LaFeO_3$_4h, (i) $LaFeO_3$_6h

Figure 2 shows a series of images obtained using transmission electron microscopy (TEM) and the elemental composition of $LaFeO_3$ samples after annealing for different time intervals: 2, 4, and 6 hours. After 2 hours of annealing, weakly agglomerated nanoparticles with irregular shapes are visible (Fig. 2 a, b, and c).

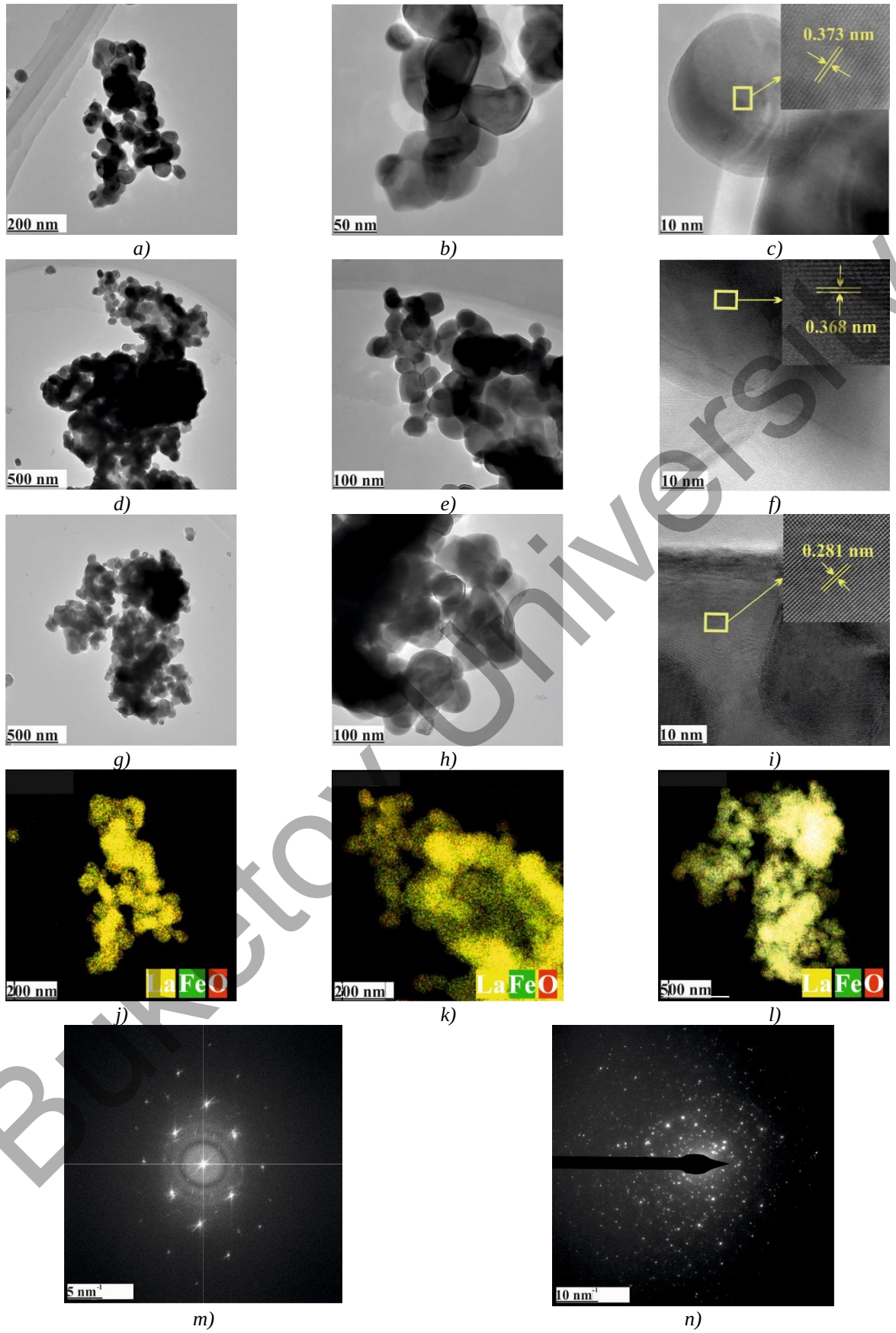

Fig.2. TEM of $LaFeO_3$ perovskite nanoparticles (a,b,c) $LaFeO_3$_2h, (d,e,f) $LaFeO_3$_4h, (g,h,i) $LaFeO_3$_6h and elemental composition (j) $LaFeO_3$_2h, (k) $LaFeO_3$_4h, (l) $LaFeO_3$_6h and electron diffraction patterns (m,n)

The particles appear to be amorphous or poorly crystallized. The particles remain relatively large, but their boundaries are still blurred, indicating insufficient crystallization. $LaFeO_3$ after annealing for 4 hours, a higher degree of particle agglomeration is observed, and the particles themselves have become more ordered compared to samples annealed for 2 hours. The particles become more uniform in size and shape. The boundaries of the particles are better distinguishable, which indicates a higher degree of crystallization. At high magnification (Figure 2f), the crystal structure characteristic of perovskite with pronounced atomic planes is clearly visible. This indicates an improvement in crystallinity compared to samples annealed for 2 hours. $LaFeO_3$ after 6 hours of annealing, the samples continue to exhibit agglomeration, but the particles become more compact and less porous (Figure 2 g, h, and i). The particles achieve greater uniformity in size, with clear boundaries, which indicates an improvement in crystallinity. A clear crystal structure is visible, with well-defined atomic planes, which confirms a high degree of crystallization during longer annealing. Electron diffraction patterns are shown in Figure 2m and 2n. The distribution of the elements La, Fe and O in each of the samples is shown in Figure 2 j, k, l. At all stages of annealing, a relatively uniform distribution of elements is observed, which confirms the successful formation of $LaFeO_3$ phases.

The X-ray diffraction (XRD) graph shown in Figure 3a demonstrates changes in the crystal structure of $Lafeo_3$ perovskite at different annealing durations of 2, 4 and 6 hours. $LaFeO_3$ perovskite is characterized by specific diffraction angles corresponding to its crystallographic planes, such as (101), (121), (220), (202), (141), (240), (242), (204). After two hours of $LaFeO_3$ annealing, diffraction peaks are observed, indicating the beginning of crystallization of the material. However, these peaks are relatively wide and have low intensity, which indicates the small size of the crystallites and the presence of structural defects. In this state, the crystals have not yet fully formed, and a significant part of the material may remain amorphous or not fully crystallized. Compared to 2-hour annealing, 4-hour annealing results in a noticeable improvement in the crystal structure. The peaks become narrower and more intense, which indicates an increase in the size of the crystallites and a decrease in the number of defects. The structure becomes more ordered, and the material undergoes a stage of active crystallization, with a better distribution of atoms in the lattice. The sample subjected to 6-hour annealing shows an even higher degree of crystallinity. The peaks on the chart become the narrowest and most intense among all three samples. This indicates that the material has reached a high level of crystalline ordering, and the crystallites have grown to significant sizes. Defects in the structure are minimized, and the material has acquired a stable crystal lattice.

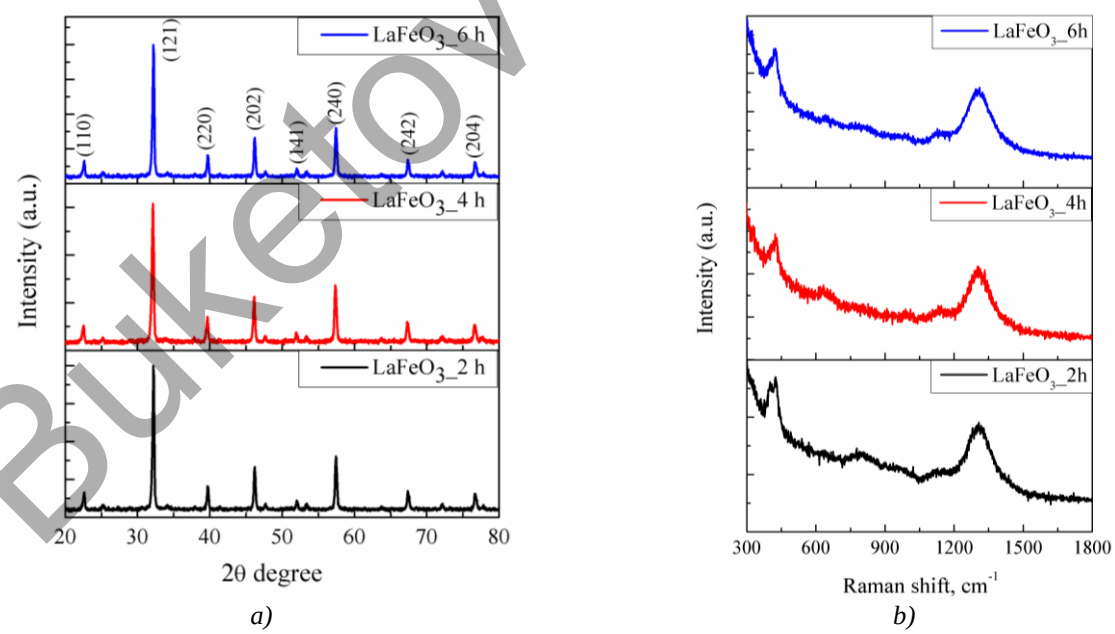

Fig.3. X-ray diffraction (a) and Raman spectroscopy (b) of $LaFeO_3$ perovskite.

With increasing annealing time, there is a noticeable narrowing of peaks on the XRD graph. This indicates an increase in the size of crystallites and an improvement in the ordering of atoms in the lattice. The intensity of the diffraction peaks also increases as the annealing time increases. This is due to the reduction of defects

and improvement of crystallinity. Two—hour annealing is characterized by the weakest peaks, whereas six-hour annealing is characterized by the most intense, which indicates a high degree of order in the structure.

As a result of prolonged annealing, the structure of $LaFeO_3$ becomes more ordered, which is expressed in increased intensity and sharpness of peaks. Samples annealed for 4 and 6 hours demonstrate significantly better crystalline properties compared to two-hour annealing, which indicates that a long heat treatment time contributes to the formation of a stable and homogeneous crystal lattice.

Figure 3b shows three graphs of Raman spectroscopy demonstrating the dependence of intensity (in arbitrary units, a.u.) on the Raman shift (in cm^{-1}) for samples of $LaFeO_3$ (lanthanum ferrite) subjected to heat treatment for 2, 4 and 6 hours. The main characteristic peaks of $LaFeO_3$ are observed in the region of 450 cm^{-1} and 1350 cm^{-1}. The annealing duration directly affects the crystal structure of $LaFeO_3$. With increasing processing time, the material gradually crystallizes, which manifests itself in clearer and more intense peaks in the Raman spectra. The sample processed for 6 hours shows the highest degree of crystallization, with pronounced peaks and high intensity. This indicates a more perfect crystal lattice compared to other samples. $LaFeO_3$ treated for 4 hours shows an intermediate degree of crystallization. Peaks are present, but their intensity and clarity are lower than in the 6-hour sample, indicating a transitional phase. Compared with the rest of the samples, $LaFeO_3$ treated for 2 hours demonstrates the initial stage of crystallization or the presence of a significant amorphous phase. The peaks are wide and weakly pronounced, which indicates that the material has not yet reached a high degree of crystallinity. Longer processing leads to an improvement in the crystal structure, with a transition from an amorphous or polycrystalline phase to a more ordered phase. This can be seen by the improvement in the intensity and clarity of peaks in the spectrum.

Figure 4 shows a graph of the absorption spectrum for samples of $LaFeO_3$ treated for different times: 2, 4 and 6 hours, the absorption peak of lanthanum ferrite is observed at about 300–500 nm. $LaFeO_3$_2h has the lowest absorption compared to the rest of the samples. $LaFeO_3$_4h shows higher absorption compared to the 2-hour sample, and $LaFeO_3$_6h also has a pronounced peak in the range of 300-500 nm. With increasing processing time (from 2 to 6 hours), the absorption of light in the visible range increases. This may indicate an improvement in the crystal structure or an increase in particle size, which leads to more efficient light absorption.

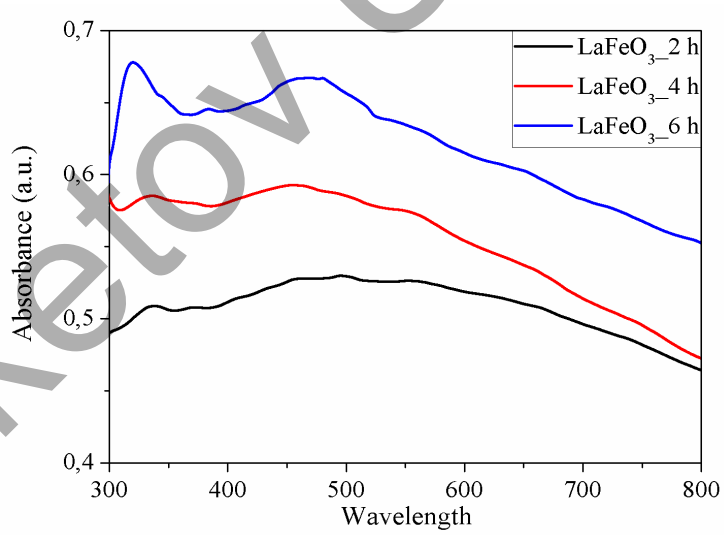

Fig.4. Absorption spectrum of $LaFeO_3$ perovskite.

The figure 5a shows the $LaFeO_3$ adsorption-desorption isotherm obtained under various heat treatment conditions (2, 4 and 6 hours) depending on the relative pressure P/P_0. All three samples show the presence of a hysteresis loop, which means the difference between sorption and desorption processes characteristic of porous materials. Hysteresis indicates the presence of capillary condensation in mesopores. At high pressure areas (P/P_0 >0.8) there is a sharp increase in adsorption for all samples, which is associated with pore filling. The sample with a longer annealing time $LaFeO_3$_6h shows the most pronounced growth, which indicates a more developed porous structure.

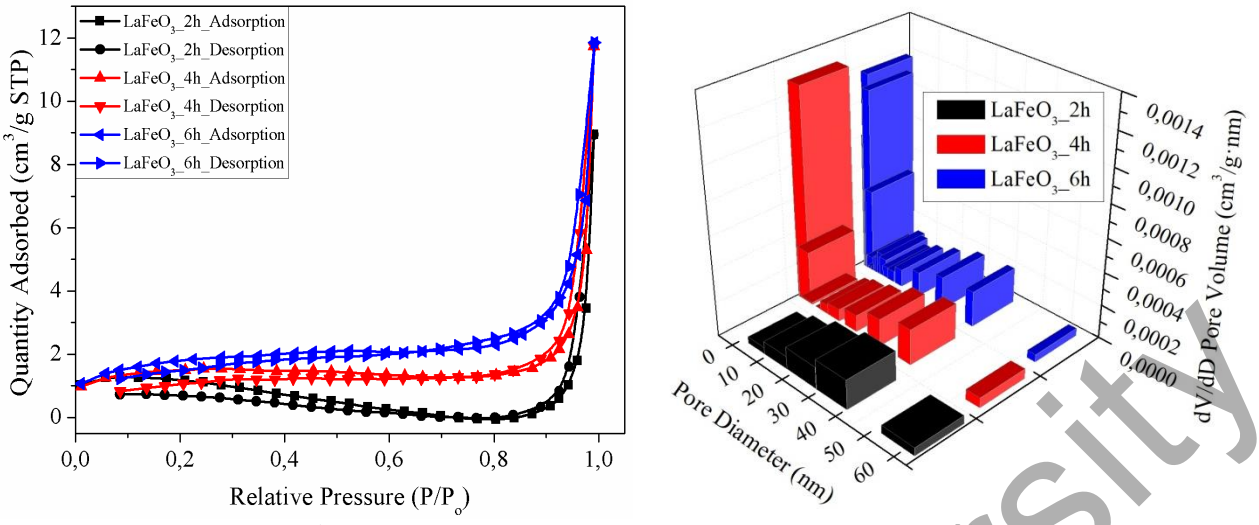

a) *b)*

Fig.5. N_2 adsorption–desorption isotherms (a) and pore size distribution curves (b) of $LaFeO_3$ perovskite.

The distribution of the pore volume depending on their diameter is presented for three samples of $LaFeO_3$ subjected to heat treatment for 2, 4 and 6 hours in Figure 5b. This is a three-dimensional diagram that illustrates how the pore volume changes (along the z axis) at different pore diameters (along the x axis) for each of the samples. In $LaFeO_3$_2h, the pore volume is relatively small compared to other samples, indicating a less developed pore system. The greatest development of the porous structure among all three samples is shown by $LaFeO_3$_6h. In this regard, it was found that an increase in the annealing time leads to an expansion of the pore distribution and an increase in their volume.

Figure 6 shows the change in current density as a function of time for samples of $LaFeO_3$ annealed for 2, 4 and 6 hours. The current density increases with increasing annealing time. The $LaFeO_3$ sample annealed for 6 hours shows the highest current density, which suggests that a longer annealing time leads to better photocatalytic activity.

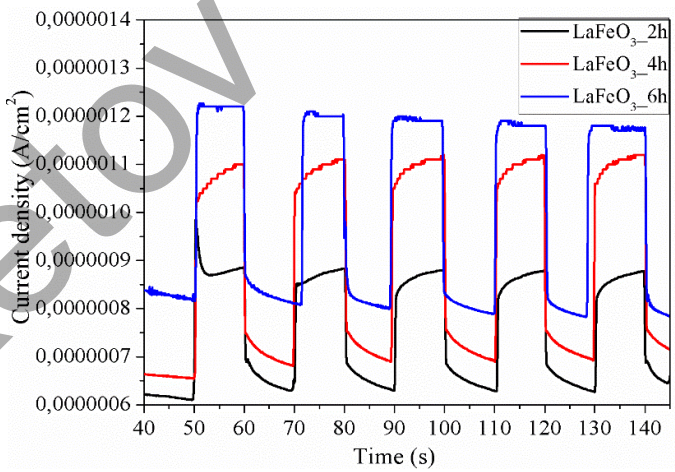

Fig.6. Photocurrent density for $LaFeO_3$ perovskite.

4. Conclusions

In the course of the study, it was found that the duration of annealing has a significant effect on the structural and photocatalytic properties of $LaFeO_3$ perovskite. The $LaFeO_3$ synthesized by the hydrothermal method demonstrates significant changes in morphology and crystal structure with increasing annealing time. Morphological changes in the material also have a significant impact on its catalytic properties. The transition from agglomerated nanoparticles to more uniform and well-formed microspheres with a smooth surface improves light absorption and interaction with reagents on the surface of the material. Experimental results have shown that an increase in the duration of annealing leads to an improvement in the crystallinity of the material, an increase in the size of crystallites and an increase in oxygenation. The improvement of the crystal structure leads to a better distribution of charges inside the material, which prevents their recombination and

thereby increases the photocatalytic activity. The highest rates of photocatalytic activity were achieved during annealing for 6 hours, which is associated with the highest degree of crystallization and improvement of the structure of the material. This study confirms the importance of controlling the heat treatment time to optimize the properties of perovskite materials, which opens up new prospects for their use as effective photocatalysts.

Conflict of interest statement

The authors declare that they have no conflict of interest in relation to this research, whether financial, personal, authorship or otherwise, that could affect the research and its results presented in this paper.

CRediT author statement: Zhanbirbayeva P.A.: Methodology, Writing - Review & Editing, Baltabekov A.S.: Writing- Original draft preparation, Kayumova A.S.: Visualization, Kuanyshbekova A.B.: Data Curation, Adambay T.N.: Data Curation, Serikov T.M.: Conceptualization, Writing - Review & Editing.
The final manuscript was read and approved by all authors.

Acknowledgments

This study was supported by the Ministry of Education and Science of the Republic of Kazakhstan (project AP23487860).

References

1 Marschall R. (2014) Semiconductor composites: strategies for enhancing charge carrier separation to improve photocatalytic activity. *Advanced Functional Materials,* 24, 2421–2440. DOI: 10.1002/adfm.201303214.

2 Boyjoo Y., Sun H., Liu J., Pareek V.K., Wang S. (2017) A review on photocatalysis for air treatment: From catalyst development to reactor design. *Chemical Engineering Journal,* 310, 537– 559. DOI:10.1016/j.cej.2016.06.090.

3 Humayun M., Qu Y., Raziq F., Yan R., Li Z., Zhang X., Jing L. (2016) Exceptional Visible-Light Activities of TiO_2-Coupled N-Doped Porous Perovskite $LaFeO_3$ for 2,4-Dichlorophenol Decomposition and CO_2 Conversion. *Environmental Science and Technology,* 50 (24), 13600-13610. DOI:10.1021/acs.est.6b04958.

4 Li J., Li H., Zhan G., Zhang L. (2016) Solar Water Splitting and Nitrogen Fixation with Layered Bismuth Oxyhalides. *Accounts of Chemical Research,* 50 (1), 112-121. DOI: 10.1021/acs.accounts.6b00523.

5 Kumar A., Sharma P., Sharma G., Dhiman P., Shekh M., Sillanpää M., Stadler F.J. (2024) Recent progress in advanced strategies to enhance the photocatalytic performance of metal molybdates for H_2 production and CO_2 reduction. *Journal of Alloys and Compounds,* 971. DOI:10.1016/j.jallcom.2023.172665.

6 Paramasivam I., Jha H., Liu N., Schmuki P. (2012) A Review of Photocatalysis using Self-organized TiO_2 Nanotubes and Other Ordered Oxide Nanostructures. *Journal of Photochemistry and Photobiology C,* 13, 1–29. DOI: 10.1002/smll.201200564.

7 Wang X., Liao M., Zhong Y., Zheng J.Y., Tian W., Zhai T., Zhi C., Ma Y., Yao J., Bando Y., Golberg D. (2012) ZnO hollow spheres with double-yolk egg structure for high-performance photocatalysts and photodetectors. *Advanced Materials,* 24 (26), 3421–3425. DOI: 10.1002/adma.201201139.

8 Liu S., Huang G., Yu J., Ng T.W., Yip H.Y., Wong P.K. (2014) Porous Fluorinated SnO_2 Hollow Nanospheres: Transformative Self-assembly and Photocatalytic Inactivation of Bacteria. *ACS Applied Materials & Interfaces,* 6 (5), 2407–2414. DOI: 10.1021/am4047975.

9 Zhang H., Li H., Wang Z., Zheng Z., Wang P., Liu Y., Zhang X., Qin X., Dai Y., Huang B. (2018) Fabrication of $BiVO_4$ photoanode consisted of mesoporous nanoparticles with improved bulk charge separation efficiency. *Applied Catalysis B: Environmental,* 238, 586–591. DOI: 10.1016/j.apcatb.2018.07.050.

10 Li Z., Qu Y., Hu K., Humayun M., Chen S., Jing L. (2017) Improved photoelectrocatalytic activities of BiOCl with high stability for water oxidation and MO degradation by coupling RGO and modifying phosphate groups to prolong carrier lifetime. *Applied Catalysis B: Environmental,* 203, 355–362. DOI: 10.1016/j.apcatb.2016.10.045.

11 Humayun M., Xu L., Zhou L., Zheng Z., Fu Q., Luo W. (2018) Exceptional co-catalyst free photocatalytic activities of B and Fe co-doped $SrTiO_3$ for CO_2 conversion and H_2 evolution. *Nano Research,* 11, 6391–6404. DOI:10.1007/s12274-018-2164-z.

12 Reyes-Gil K.R., Wiggenhorn C., Brunschwig B.S., Lewis N.S. (2013) Comparison between the Quantum Yields of Compact and Porous WO_3 Photoanodes. *The Journal of Physical Chemistry C,* 117 (29), 14947–14957.

13 Zhou X., Xu Q., Lei W., Zhang T., Qi X., Liu G., Deng K., Yu J. (2014) Origin of Tunable Photocatalytic Selectivity of Well-Defined α-Fe_2O_3. *Nanocrystals,* 10 (4), 674–679. DOI: 10.1002/smll.201301870.

14 Sakamoto H., Ohara T., Yasumoto N., Shiraishi Y., Ichikawa S., Tanaka S., Hirai T. (2015). Hot-Electron-Induced Highly Efficient O_2 Activation by Pt Nanoparticles Supported on Ta_2O_5 Driven by Visible Light. *Journal of the American Chemical Society,* 137 (27), 9324–9332. DOI: 10.1021/jacs.5b04062.

15 Humayun M., Zada A., Li Z., Xie M., Zhang X., Qu Y., Raziq F., Jing L. (2016) Enhanced visible-light activities of porous $BiFeO_3$ by coupling with nanocrystalline TiO_2 and mechanism. *Applied Catalysis B: Environmental*, 180, 219–226. DOI: 10.1016/j.apcatb.2015.06.035.

16 Xie M., Feng Y., Fu X., Luan P., Jing L. (2015) Phosphate-bridged TiO_2–$BiVO_4$ nanocomposites with exceptional visible activities for photocatalytic water splitting. *Journal of Alloys and Compounds*, 631, 120–124. DOI:10.1016/j.jallcom.2015.01.091.

17 An X., Li K., Tang J. (2014) Cu_2O/Reduced Graphene Oxide Composites for the Photocatalytic Conversion of CO_2. *ChemSusChem.*, 7 (4), 1086–1093. DOI: 10.1002/cssc.201301194.

18 Xing W., Tu W., Han Z., Hu Y., Meng Q., Chen G. (2018) Template-Induced High-Crystalline g-C_3N_4 Nanosheets for Enhanced Photocatalytic H_2 Evolution. *ACS Energy Letters*, 3 (2), 514–519.

19 Zhang F., Li Y.-H., Li J.-Y., Tang Z.-R., Xu Y.-J. (2019) 3D graphene-based gel photocatalysts for environmental pollutants degradation. *Environmental Pollution*, 253, 365–376. DOI: 10.1016/j.envpol.2019.06.089.

20 Ge J., Zhang Y., Park S.-J. (2019) Recent Advances in Carbonaceous Photocatalysts with Enhanced Photocatalytic Performances: A Mini Review. *Materials*, 12, 1916. DOI: 10.3390/ma12121916.

21 Khan N.A., Humayun M., Usman M., Ghazi Z.A., Naeem A., Khan A.L., Khan A.A., Tahir A.A., Ullah H. (2021) Structural Characteristics and Environmental Applications of Covalent Organic Frameworks. *Energies*, 14 (8), 2267. DOI: 10.3390/en14082267.

22 Yaseen M., Humayun M., Khan A., Usman M., Ullah H., Tahir A.A., Ullah H. (2021) Preparation, Functionalization, Modification, and Applications of Nanostructured Gold: A Critical Review. *Energies*, 14 (5), 1278. DOI:10.3390/en14051278.

23 Ashraf M., Khan I., Usman M., Khan A., Shah S.S., Khan A.Z., Saeed K., Yaseen M., Ehsan M.F., Tahir M.N., Ullah N. (2020) Hematite and Magnetite Nanostructures for Green and Sustainable Energy Harnessing and Environmental Pollution Control: A Review. *Chemical Research in Toxicology*, 33 (5), 1292–1311. DOI: 10.1021/acs.chemrestox.9b00308.

24 Tijare S.N., Joshi M.V., Padole P.S., Mangrulkar P.A., Rayalu S.S., Labhsetwar N.K. (2012) Photocatalytic hydrogen generation through water splitting on nano-crystalline $LaFeO_3$ perovskite. *International Journal of Hydrogen Energy*, 37 (13), 10451–10456. DOI: 10.1016/j.ijhydene.2012.01.120.

25 Jiang Y., Lv Q., Xu F., Sun X., Ding Y. (2021) Synthesis of TiO_2/$LaFeO_3$ composites for the photoelectrochemical hydrogen evolution. *Journal of Materials Science*, 56 (26), 15188–15204. DOI:10.1007/s10853-021-06188-3.

26 Assirey E.A.R. (2019) Perovskite synthesis, properties and their related biochemical and industrial application. *Saudi Pharmaceutical Journal*, 27 (6), 817–829. DOI: 10.1016/j.jsps.2019.05.003.

27 Thirumalairajan S., Girija K., Ganesh I., Mangalaraj D., Viswanathan C., Balamurugan A., Ponpandian N. (2013) Controlled synthesis of perovskite $LaFeO_3$ microsphere composed of nanoparticles via self-assembly process and their associated photocatalytic activity. *Journal of Physical Chemistry C*, 117 (8), 3219–3227. DOI:10.1016/j.cej.2012.08.012.

AUTHORS' INFORMATION

Zhanbirbayeva, Perizat Amangeldievna - Doctoral student, Karaganda University named after academician E.A. Buketov, Karaganda, Kazakhstan. Scopus Author ID: 58091458000, ORCID iD: 0000-0002-9351-956X, perizat.zhanbirbaeva@mail.ru

Baltabekov, Askhat Sekerbaevich - PhD, associate professor, Karaganda University named after academician E.A. Buketov, Karaganda, Kazakhstan. Scopus Author ID: 35193461600, ORCID iD: 0000-0001-8829-2527, abskargu@mail.ru

Kayumova, Ainur Serikovna - Doctoral student, Karaganda University named after academician E.A. Buketov, Karaganda, Kazakhstan. Scopus Author ID: 58547258400, ORCID iD: 0000-0003-4684-0083, aneka.08@mail.ru

Kuanyshbekova, Ayazhan Bakhtiyarovna – Magistr, Karaganda University named after academician E.A. Buketov, Karaganda, Kazakhstan. ORCID iD: 0009-0002-7300-868X, kuanyshbekovaaya@mail.ru

Adambay, Tolganay Nurbolatkyzy – Student, Karaganda University named after academician E.A. Buketov, Karaganda, Kazakhstan. ORCID iD: 0009-0009-8127-8090, adambay.tolganay@mail.ru

Serikov, Timur Maratovich - PhD, associate professor, Karaganda University named after academician E.A. Buketov, Karaganda, Kazakhstan. Scopus Author ID: 56669712000, ORCID iD: 0000-0003-4302-9674, serikov-timur@mail.ru